Journal of Power Sources 196 (2011) 5645–5650

Contents lists available at ScienceDirect

Journal of Power Sources

journal homepage: www.elsevier.com/locate/jpowsour

$(NH_4)_{0.5}V_2O_5$ nanobelt with good cycling stability as cathode material for Li-ion battery

Haiyan Wang[a], Kelong Huang[a,*], Chenghuan Huang[a], Suqin Liu[a], Yu Ren[b], Xiaobing Huang[c]

[a] School of Chemistry and Chemical Engineering, Central South University, Changsha 410083, China
[b] EaStChem and School of Chemistry, University of St Andrews, St Andrews, Fife KY16 9ST, UK
[c] Chengdu Institute of Organic Chemistry, Chinese Academy of Science, Chengdu 610041, China

ARTICLE INFO

Article history:
Received 1 November 2010
Received in revised form 11 January 2011
Accepted 17 February 2011
Available online 24 February 2011

Keywords:
Li-ion battery
Ammonium divanadate nanobelt
Hydrothermal method
Sodium dodecyl benzene sulfonate
Electrochemical performance

ABSTRACT

$(NH_4)_{0.5}V_2O_5$ nanobelt is synthesized by sodium dodecyl benzene sulfonate (SDBS) assisted hydrothermal reaction as a cathode material for Li-ion battery. The as-prepared $(NH_4)_{0.5}V_2O_5$ nanobelts are 50–200 nm in diameter and several micrometers in length. The reversible lithium intercalation behavior of the nanobelts has been evaluated by cyclic voltammetry, galvanostatic discharge–charge cycling, and electrochemical impedance spectroscopy. The $(NH_4)_{0.5}V_2O_5$ delivers an initial specific discharge capacity of 225.2 mAh g^{-1} between 1.8 and 4.0 V at 15 mA g^{-1}, and still maintains a high discharge capacity of 197.5 mAh g^{-1} after 11 cycles. It shows good rate capability with a discharge capacity of about 180 mAh g^{-1} remaining after 40 cycles at various rates and excellent cycling stability with the capacity retention of 81.9% after 100 cycles at 150 mA g^{-1}. Interestingly, the excess 120 mAh g^{-1} capacity in the first charge process is observed, most of which could be attributed to the extraction of NH_4^+ group, verified by Fourier transform Infrared (FT-IR) and X-ray diffraction (XRD) results.

1. Introduction

Vanadium oxides and their derivative compounds have attracted much attention as cathode materials for Li-ion battery due to their high discharge capacity and low cost [1–12]. Among them, lithium trivanadate ($Li_{1+x}V_3O_8$), is considered a very promising one. However, it should be noted that the preparation method as well as post-treatment condition could strongly affect the electrochemical properties of this material [7,8]. LiV_3O_8 prepared by traditional solid state method showed a low discharge capacity of 180 mAh g^{-1} [6]. Liu et al. [10] fabricated single-crystalline LiV_3O_8 nanorods, exhibiting an initial discharge capacity of 348 mAh g^{-1} at 20 mA g^{-1}. Nanosize electrode material can provide not only short diffusion pathway for lithium ion intercalation/de-intercalation in host material, but also high specific surface area, which permits a high contact area with electrolyte and hence a high Li^+ flux across the interface [13].

Hydrothermal method has been widely used to synthesize lithium intercalation materials with various nanomorphologies (nanorod [8,14], nanowire [15,16] and nanobelt [17,18], etc.). However, to the best of our knowledge, no LiV_3O_8 could be obtained by one-step hydrothermal method. Recently, we reported a new cathode material $NH_4V_3O_8{\cdot}0.2H_2O$ by one-step hydrothermal method, which delivered a maximum discharge capacity of 225.9 mAh g^{-1} with good cycling stability [19]. $NH_4V_3O_8$ is isostructure of LiV_3O_8, with $V_3O_8^-$ layers stacked along the *c*-direction and the NH_4^+ cations occupying the interlayer space [20]. The high discharge capacity of LiV_3O_8, as well as $NH_4V_3O_8$ is due to the new lithium ion insertion from lithium metal anode [19,21]. That is, Li^+ in LiV_3O_8 and NH_4^+ groups in $NH_4V_3O_8$ probably act as pillars to stabilize the layer structure. So, it stimulates a new direction using ammonium vanadate instead of lithium vanadate, as cathode material for lithium ion battery [19].

Accordingly, in the present work, we describe a facile, large-scale hydrothermal method to fabricate another ammonium vanadate, namely $(NH_4)_{0.5}V_2O_5$ (also can be written as $NH_4V_4O_{10}$) nanobelt for Li-ion battery. Recently, $(NH_4)_{0.5}V_2O_5$ has been synthesized by several groups [22–24]. However, only Zhang and co-workers [24] reported the electrochemical properties of $NH_4V_4O_{10}$, which showed an initial discharge capacity of 171.8 mAh g^{-1} and poor cycling performance, with less than 80 mAh g^{-1} after 17 cycles. Obviously, much more work is necessary to improve its cycling stability for application in Li-ion battery. Herein, we demonstrate the $(NH_4)_{0.5}V_2O_5$ nanobelt with excess 220 mAh g^{-1} initial discharge capacity and excellent cycling stability. The charge–discharge mechanism is also discussed in detail.

* Corresponding author. Tel.: +86 731 88879850; fax: +86 731 88879850.
E-mail address: klhuang@mail.csu.edu.cn (K. Huang).

0378-7753/$ – see front matter © 2011 Published by Elsevier B.V.
doi:10.1016/j.jpowsour.2011.02.046

2. Experimental

2.1. Synthesis of $(NH_4)_{0.5}V_2O_5$ nanobelts

All the starting materials were analytically pure grade. In this work, sodium dodecyl benzene sulfonate (SDBS) was used as a soft template. At first, 1.755 g NH_4VO_3 and 1.045 g SDBS were dissolved in deionized water successively. Then a proper amount of hydrochloric acid with the concentration of 1.2 mol l^{-1} was added into the solution to adjust the pH value to about 1.0. The mixed solution was then transferred into a 50 ml Teflon lined stainless steel autoclave. The total volume of the solution was about 40 ml. The autoclave was sealed and heated at 180 °C for 24 h and then cooled to room temperature naturally. The obtained precipitate was filtered, washed with deionized water three times. Finally, the product was obtained by drying the precipitates at 80 °C overnight.

2.2. Characterization

Powder X-ray diffraction (XRD) data were obtained by a Philips X-Pert system (Cu-Kα radiation) with a step of 0.02°. Infrared (IR) absorption spectra were recorded using the Nicolet 6700 Fourier transform infrared (FT-IR) spectrometer. Morphological studies were conducted using a JEOL JEM-2011 transmission electron microscopy (TEM), employing a LaB6 filament as the electron source and an accelerating voltage of 200 keV. N_2 adsorption–desorption analysis was carried out using a Micromeritics ASAP 2020. The typical sample weight used was about 100 mg. The outgas condition was set to 180 min at 120 °C under vacuum, and all adsorption–desorption measurements were carried out at liquid nitrogen temperature. For the characterization of electrode materials after cycling by other techniques, such as XRD and FT-IR, the powder of active material was recovered from the cell followed by washing with dimethyl carbonate (DMC) several times and drying under dynamic vacuum for 2 h without exposure to air.

2.3. Electrochemical measurements

The electrochemical tested cells were constructed by mixing the active material, polytetrafluoroethylene (PTFE), and carbon black in a weight ratio of 80:10:10. The mixture was cast onto Al foil from acetone using a Doctor-Blade technique. After drying at 80 °C under vacuum for 8 h, the electrodes were assembled into CR2016 coin-type cells with a Li electrode and commercial electrolyte (Merck; 1 M $LiPF_6$ in 1:1 (v/v) ethylene carbonate/dimethyl carbonate) in an Ar-filled MBraun glove box. The cells were cycled galvanostatically between 1.8 and 4.0 V (voltage unit in this paper is versus Li/Li^+) at a desired current density with a Land tester system (CT2001A, Wuhan Land Electronic Co. Ltd.) at room temperature. Cyclic voltammetry (CV) test was carried out using the electrochemical station (Shanghai Chenhua, China) with a scan rate of 0.1 mV s^{-1} at room temperature. Electrochemical impedance spectroscopy (EIS) was recorded by the Solartron analytical instrument over the frequency range from 500 kHz to 10 mHz with an amplitude of 5 mV. Before testing, the cell was charged to 2.6 V and then kept at that voltage for 2 h.

3. Results and discussion

The as-prepared powder is single phase $NH_4V_4O_{10}$ (JCPDS Card No.31-0075) as determined by XRD (Fig. 1). It can be indexed into a monocline structure with the lattice parameters of $a = 1.174$ nm, $b = 0.369$ nm, $c = 0.998$ nm and $\beta = 98.85°$, which are a little different from those reported in the literatures [23,24]. The as-prepared

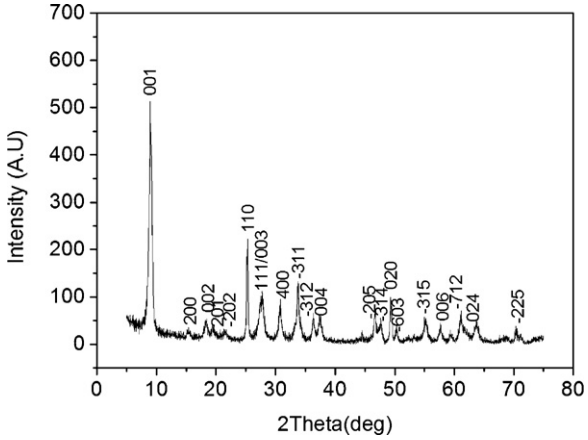

Fig. 1. XRD pattern of the as-prepared powder.

$(NH_4)_{0.5}V_2O_5$ in this report indicates a little larger unit cell volume (0.4272 nm^3) than that (0.4017 nm^3) in Ref. [24] ($a = 1.166$ nm, $b = 0.361$ nm, $c = 0.971$ nm and $\beta = 100.6°$), which probably provides more flexible pathway for lithium ion transport, and further influences the electrochemical performance.

The FT-IR spectrum of the $(NH_4)_{0.5}V_2O_5$ powder is depicted in Fig. 2. As can be seen, the sample indicates the bands at about 3199.5, 1423.2, 999.6, 941.7, 748.1 and 531.7 cm^{-1}, respectively. The bands at 999.6 and 941.7 cm^{-1} are due to V=O stretching of distorted octahedral and distorted squarepyramids, while those at 748.1 and 531.7 cm^{-1} can be assigned to asymmetric and symmetric stretching vibration of V–O–V bonds [25]. Moreover, the bands at 3199.5 and 1423.2 cm^{-1} are attributed to the asymmetric stretching vibrations and the symmetric bending vibration of NH_4^+ [26]. In our previous work [19], it was found that crystallographic water in $NH_4V_3O_8{\cdot}0.2H_2O$ affected its structure, probably further affected the electrochemical performance. Wu et al. [23] reported that there was crystallographic water in $(NH_4)_{0.5}V_2O_5$ due to the existence of the adsorption band at 3418.1 cm^{-1} in IR curve. For $(NH_4)_{0.5}V_2O_5$ reported in this work, it does not exhibit such evidence, inferring it is a pure $(NH_4)_{0.5}V_2O_5$ phase without crystallographic water.

Fig. 3 shows TEM images of as-prepared $(NH_4)_{0.5}V_2O_5$ powder under different magnifications. As observed, this material is of belt-like shape with the 50–200 nm width and several micrometers length. Obviously, some of the primary belts are partially attached together to form larger and wider ones. The BET surface area of the $(NH_4)_{0.5}V_2O_5$ nanobelts is about 27 m^2 g^{-1}. It is well known that particle size and morphology of electrode materials are very impor-

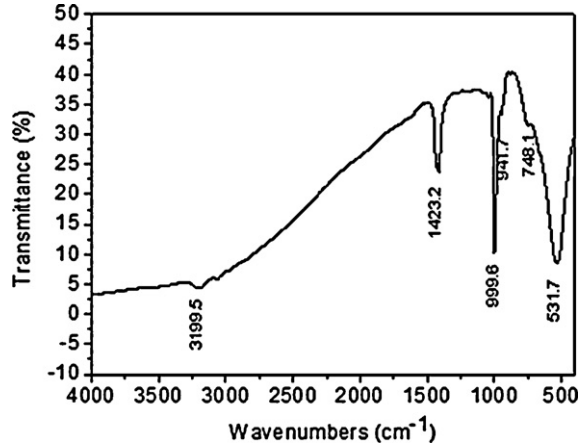

Fig. 2. Fourier transform infrared spectrum of $(NH_4)_{0.5}V_2O_5$ powder.

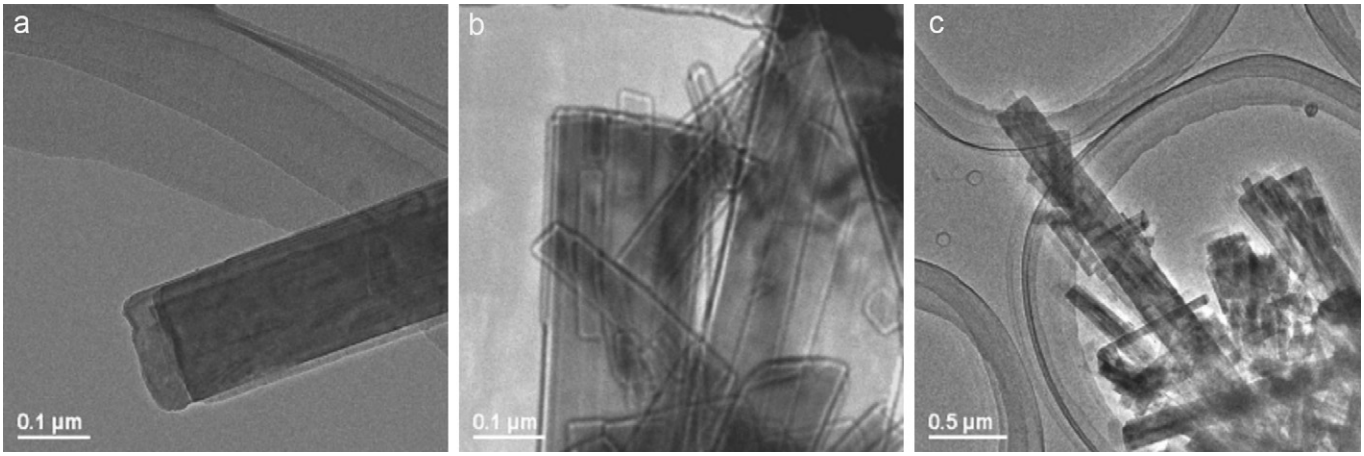

Fig. 3. TEM images under different magnifications of $(NH_4)_{0.5}V_2O_5$ powder.

tant for their electrochemical performance in Li-ion battery [12]. In this paper, nano-belt morphology will provide better electrochemical property for layered compound $(NH_4)_{0.5}V_2O_5$ electrode since the intercalation and de-intercalation of Li^+ between the layers of cathode should be a diffusion process [12].

Fig. 4 shows the specific discharge capacity versus cyclic numbers of $(NH_4)_{0.5}V_2O_5$ nanobelts at a current density of 15 mA g^{-1} between 1.8 and 4.0 V. The inset image is the first 11 galvanostatic discharge curves with no noticeable capacity fading, inferring that lithium ion can highly reversibly insert into and extract from the host material. $(NH_4)_{0.5}V_2O_5$ nanobelts give an initial specific discharge capacity of 225.2 mAh g^{-1} (about 1.6 electrons per unit formula are exchanged) and the discharge capacity of 197.5 mAh g^{-1} at the 11th cycle. It shows much better capacity retention in comparison with the previous report [24]. The related explanation is shown in the following text. Undoubtedly, the specific discharge capacity of $(NH_4)_{0.5}V_2O_5$ is higher than that of LiV_3O_8 prepared by ordinary solid state method [7] and comparable to layered lithium transition metal oxides (e.g., $LiMnO_2$, $LiNi_{1/3}Co_{1/3}Mn_{1/3}O_2$, etc.) [27,28]. It is worth mentioning that there is a large capacity loss during the first three cycles and then the discharge capacity keeps stable, which is probably resulted from the slight structure rearrangement due to the new lithium ions insertion. The phenomenon above is different from that of $NH_4V_3O_8$ reported in our previous work [19], which presented the gradual improved discharge capacity for the first several cycles. From the inset galvanostatic discharge curves, there are three discharge voltage plateaus at about 2.52 V, 2.83 V and 3.69 V, respectively. The discharge capacity loss mainly results from the plateaus at about 2.52 V. The CV curves (Fig. 5) were measured to investigate the change of discharge capacity for the first three cycles. Three pairs of redox peaks, with the oxidation peaks located at about 2.69 V, 2.91 V, 3.71 V and the corresponding reduction peaks at about 2.47 V, 2.80 V, 3.65 V respectively, are observed. Appearance of redox peaks indicates the reversible Li^+ de-intercalation and intercalation in solid phase. It is noted that there is also peak area loss in the first three CV curves, which is in good agreement with the trend in Fig. 4. Apparently, $(NH_4)_{0.5}V_2O_5$ nanobelt possesses good cycling stability after the first two cycles.

The rate capability of $(NH_4)_{0.5}V_2O_5$ nanobelts is also investigated (Fig. 6). The tested cell was continuously carried out 5 cycles at various current densities, ranging from 30 mA g^{-1} to 450 mA g^{-1}, then further measured 20 cycles at 30 mA g^{-1} again. It can be seen that the electrode also displays discharge capacity loss for the first several cycles at 30 mA g^{-1}. The discharge capacity decreases with the increasing of current density. Surprisingly, no obvious capacity fading is observed after the initial capacity loss and cycling at high rates. The fifth specific discharge capacity of $(NH_4)_{0.5}V_2O_5$ electrode at 30 mA g^{-1}, 120 mA g^{-1}, 240 mA g^{-1},450 mA g^{-1} is 192.6 mAh g^{-1}, 160.1 mAh g^{-1}, 142.7 mAh g^{-1}, and 121.3 mAh g^{-1}, respectively. When cycling at 30 mA g^{-1} again, the discharge capacity recovers to 192.4 mAh g^{-1}, almost without capacity loss after cycling at various rates. The capacity fading is about 6.8% after the subsequent 20 cycles. Long cycling test (Fig. 7) was continued to

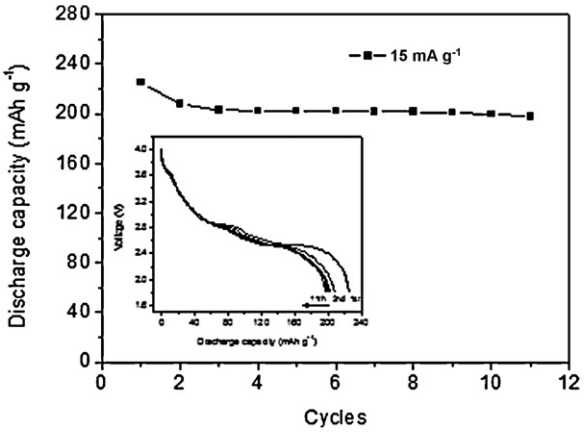

Fig. 4. Cycling performance of $(NH_4)_{0.5}V_2O_5$ operated between 1.8 and 4.0 V at a current density of 15 mA g^{-1}, together with its discharge galvanostatic curves inset.

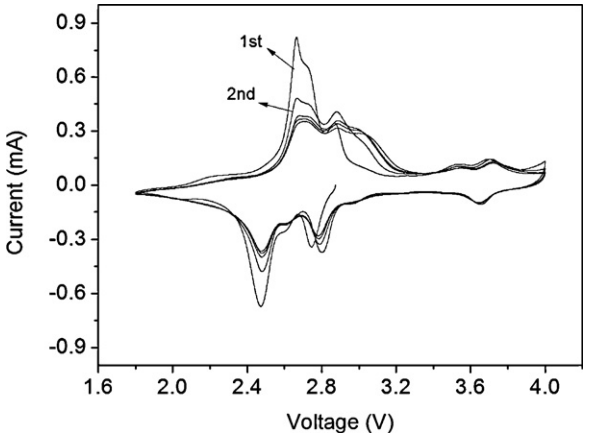

Fig. 5. Cyclic voltammetry curves of $(NH_4)_{0.5}V_2O_5$ electrode between 1.8 and 4.0 V at scanning rate 0.1 mV s^{-1}.

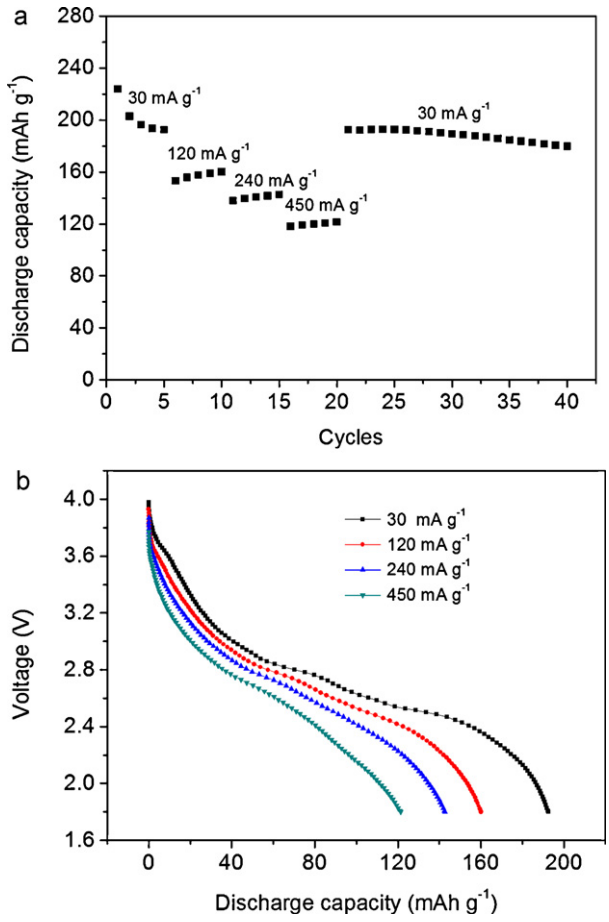

Fig. 6. (a) Cycling performance and (b) the fifth discharge curves of $(NH_4)_{0.5}V_2O_5$ electrode at various current densities (30 mA g^{-1}, 120 mA g^{-1}, 240 mA g^{-1}, 450 mA g^{-1}), between 1.8 and 4.0 V.

confirm cycling performance of $(NH_4)_{0.5}V_2O_5$ nanobelt. As indicated, the electrode exhibits the capacity retention of 81.9% after 100 cycles at a current density of 150 mA g^{-1}, although the initial discharge capacity decreases to 141.3 mAh g^{-1}. Above results reveal that $(NH_4)_{0.5}V_2O_5$ prepared in this work shows excellent cycling stability and good rate capability. Wu et al. [23] reported that the conductivity of $(NH_4)_{0.5}V_2O_5$ nanobelt was $\sim 10^{-3}$ S cm^{-1} at room temperature, which is close to that of RF-sputtered V_2O_5 ($\sigma \sim 10^{-4}$–10^{-3} S cm^{-1}) [29].

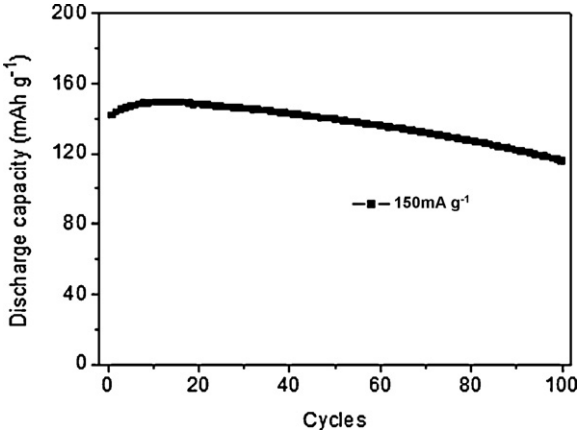

Fig. 7. Long cycling performance of $(NH_4)_{0.5}V_2O_5$ at 150 mA g^{-1} between 1.8 and 4.0 V.

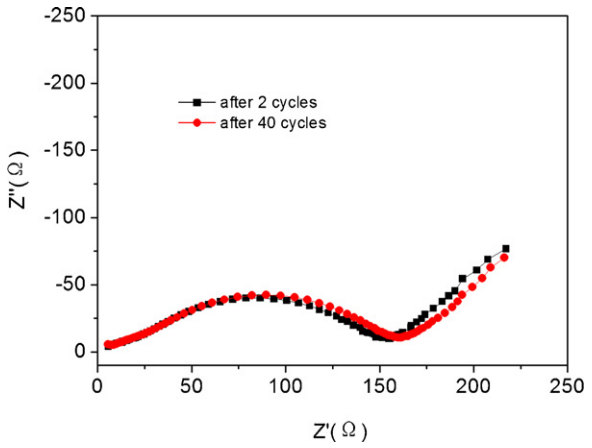

Fig. 8. Nyquist plots of the $(NH_4)_{0.5}V_2O_5$ electrode at 2.6 V after 2 and 40 cycles at various rates, shown in Fig. 6a.

To further understand the good cycling stability of $(NH_4)_{0.5}V_2O_5$ electrode, Nyquist plots at 2.6 V after different cycles (2nd, 40th in Fig. 6) at various rates are recorded in Fig. 8, respectively. As observed, each impedance spectrum consists of a depressed semicircle at the high frequency followed by a slop line at the low frequency range. It has been confirmed that the depressed semicircle is considered as the contribution of the charge-transfer process, while the slop line is due to Warburg impedance which reflects lithium ion diffusion in the solid state electrodes [30,31]. From Fig. 8, the impedance spectra of $(NH_4)_{0.5}V_2O_5$ electrode change a little, which is consistent with the cycling performance in Fig. 6a. It is noted that lithium ion diffusion coefficient could be calculated from the low frequency plots according to the following equation [32,33]:

$$D = \frac{R^2T^2}{2A^2n^4F^4C^2\sigma^2} \quad (1)$$

where R is the gas constant, T is the absolute temperature, A is the surface area of the cathode, n is the number of electrons per molecule during oxidation, F is the Faraday constant, C is the concentration of lithium ion, σ is the Warburg factor which is relative with Z' [32,33]:

$$Z' = R_D + R_L + \sigma\omega^{-1/2} \quad (2)$$

where ω is frequency. Fig. 9 illustrates the relationship curve between Z' and $\omega^{-1/2}$ in the low frequency and the Warburg factor (σ) is calculated as 6.94622 Ω cm^2 s$^{-1/2}$. Thus, according to the Eqs.

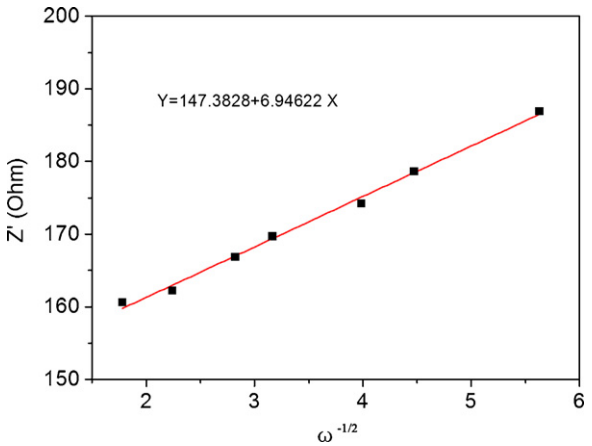

Fig. 9. The relationship curve between Z' and $\omega^{-1/2}$ in the low frequency.

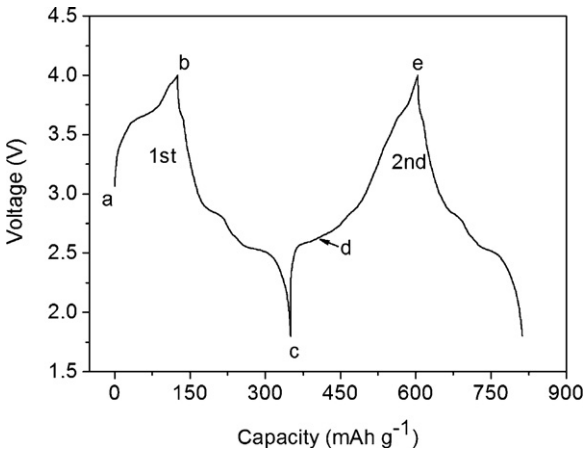

Fig. 10. The first two charge–discharge curves of $(NH_4)_{0.5}V_2O_5$ electrode between 1.8 and 4.0 V at a current density of 15 mA g^{-1}; The inset symbols of (a)–(e) depict different charge status: (a) no cycling; (b) charge to 4.0 V; (c) discharge to 1.8 V at the 1st cycle; (d) charge to 2.6 V at the 2nd cycle; (e) charge to 4.0 V at the 2nd cycle.

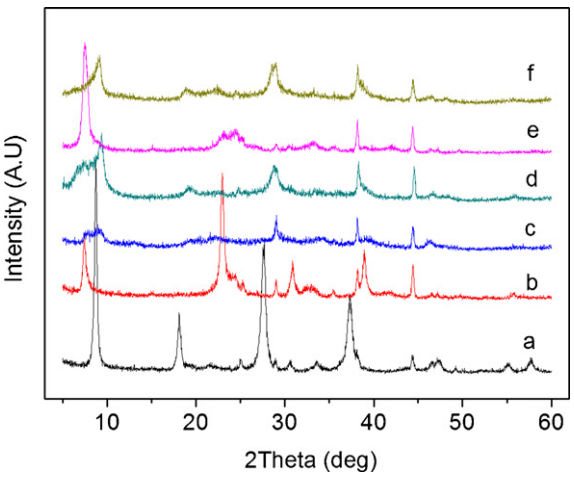

Fig. 12. XRD patterns of $(NH_4)_{0.5}V_2O_5$ electrodes at different voltages after cycling: (a) no cycling; (b) charge to 4.0 V; (c) discharge to 1.8 V at the 1st cycle; (d) charge to 2.6 V at the 2nd cycle; (e) charge to 4.0 V at the 2nd cycle; (f) charge to 2.6 V after 40 cycles at various rates, shown in Fig. 6.

(1) and (2), the lithium ion diffusion coefficient of $(NH_4)_{0.5}V_2O_5$ is about 1.89×10^{-10} cm S^{-1}, which is close to that of $LiCoO_2$ [34].

Fig. 10 depicts the first two galvanostatic charge–discharge curves of $(NH_4)_{0.5}V_2O_5$ nanobelts at 15 mA g^{-1}. Surprisingly, it delivers around 120 mAh g^{-1} capacity at the first charge process, which is not consistent with those alkaline or alkaline-earth metal trivanadium oxides, such as LiV_3O_8, NaV_3O_8 and $NH_4V_3O_8$ [5,19,21]. In trivanadium oxides, the additional alkaline ions were just arranged to form pillar between the vanadium oxide layers and thus stabilize the structure during lithium ion intercalation and de-intercalation [19]. In the case of $(NH_4)_{0.5}V_2O_5$, vanadium shows valance state of +4.75, which could be oxidized to +5 and probably accompanied with NH_4^+ group extraction. More importantly, as can be seen, there is an obvious charge plateau in the first charge during 3.6–3.7 V, which is not observed in the following charge. Herein, we speculate that a great part of the first charge capacity (unexpected side reaction in the first charge process may result in a certain amount of capacity) could be attributed to the extraction of NH_4^+ from the host material. Such hypothesis is confirmed by the comparison of the FT-IR spectra of $(NH_4)_{0.5}V_2O_5$ electrode powder charged to different voltages, as demonstrated in Fig. 11. Apparently, the bands at 3199.3 and 1406.5 cm^{-1} in both FT-IR curves are ascribed to the asymmetric stretching vibrations and the symmetric bending vibration of NH_4^+ [26], while those at 999.5 and

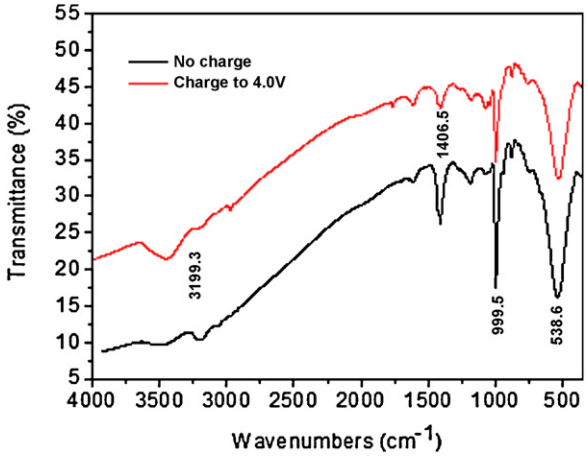

Fig. 11. FT-IR spectra of $(NH_4)_{0.5}V_2O_5$ electrode powder: (a) no charge; (b) charge to 4.0 V.

941.6 cm^{-1} are due to V=O stretching of distorted octahedral and distorted squarepyramids [25]. There is no doubt that the V=O of $(NH_4)_{0.5}V_2O_5$ is independent of charging. Therefore, the ratio of the band intensity of NH_4^+ to that of V=O could imply the behavior of NH_4^+ group during the charge process. As illustrated, the ratio of $(NH_4)_{0.5}V_2O_5$ electrode charge to 4.0 V is much less than that without charging, which should result from the decreasing amount of NH_4^+ group in bulk material. The extraction of NH_4^+ group would result in slight structure rearrangement. It is understandable that the new lithium ions would insert into the site that the former NH_4^+ group occupying in first discharging, some of which could not extract from the host and probably work as stabilizing cations as NH_4^+ did before. That is why the $(NH_4)_{0.5}V_2O_5$ electrode shows the obvious capacity loss in the first two cycles in Fig. 4. As for the transmission of NH_4^+ group in electrolyte and how to insert into Li metal anode, it is not clear in this paper so far. The mechanism will be further studied in our future work.

XRD patterns of $(NH_4)_{0.5}V_2O_5$ nanobelts at different voltages after cycling (in Fig. 10a–e) are also investigated to further understand the charge–discharge mechanism, as displayed in Fig. 12. The electrode consisting of active material, carbon and binder, after washing with DMC and dried for 2 h, was directly used to examine the structure. As observed, the electrode a shows the similar XRD pattern with as-prepared $(NH_4)_{0.5}V_2O_5$ nanobelt in Fig. 1, except intensity changes in some diffraction peaks. The phenomenon above is probably attributed to the more smooth surface of electrode film in comparison with the powder. When the fresh electrode is charged to 4.0 V, its strongest diffraction peak (0 0 1) shifts toward the low angle direction, with decreasing intensity. At the same time, some peaks at 18.2°, 27.6° and 37.3° nearly disappear and new peaks at 23.2° and 24.3° arise. Those information implies that the structure of $(NH_4)_{0.5}V_2O_5$ is changed, even though the monoclinic system is still retained, which should be due to the extraction of NH_4^+ group from the host material to form the $(NH_4)_{0.5-x}V_2O_5$ compound ($x < 0.5$ based on the FTIR results in Fig. 11). It is noted that the main diffraction peaks are further weaken with the intercalation of lithium ion (Fig. 12c), whereas no new peak appears. On the contrary, it is clearly that the diffraction peak (0 0 1) increases gradually when charging again, shown in Fig. 12d and e. Comparatively, Fig. 12f indicates the very similar diffraction peaks with Fig. 12e, which suggests that the $(NH_4)_{0.5}V_2O_5$ electrode possesses good structural stability even cycling at high current density. It agrees well with the electro-

chemical performance in Fig. 6. According to the results above, it is thereby expected that the as-prepared $(NH_4)_{0.5}V_2O_5$ nanobelt with excellent cyclic stability could be a very promising cathode material for Li-ion battery.

4. Conclusions

A new cathode material, $(NH_4)_{0.5}V_2O_5$ nanobelt with good cycling stability was synthesized. The nanobelts are of width of 50–200 nm and length up to several micrometers. The as-obtained $(NH_4)_{0.5}V_2O_5$ electrode shows good reversible lithium ion insertion and extraction ability, with the initial specific discharge capacity of 225.2 mAh g^{-1} at 15 mA g^{-1} and discharge capacity of 197.5 mAh g^{-1} remaining after 11 cycles. Meanwhile, it exhibits the discharge capacity of 192.6 mAh g^{-1}, 160.1 mAh g^{-1}, 142.7 mAh g^{-1}, 121.3 mAh g^{-1} at 30 mA g^{-1}, 120 mA g^{-1}, 240 mA g^{-1}, 450 mA g^{-1} respectively. The electrode shows obvious capacity fading in the first two cycles probably due to the slight structure reorganization because of the insertion of lithium ion. The long cycling test for 100 cycles at 150 mA g^{-1} presents the capacity retention of 81.9%. In addition, the lithium ion diffusion coefficient of $(NH_4)_{0.5}V_2O_5$ electrode is 1.89×10^{-10} cm S^{-1}. More interestingly, it is found that NH_4^+ in the host material could extract in the first charge process, as proved by the FT-IR and XRD results.

Acknowledgements

Financial Support from the Major State Basic Research Development Program of China (973 Program) (no. 2010CB227204), the National Natural Science Foundation of China (no. 50972165), Graduate Degree Thesis Innovation Foundation of Central South University (1960-71131100017) is greatly appreciated.

References

[1] A.M. Cao, J.S. Hu, H.P. Liang, L.J. Wan, Angew. Chem. Int. Ed. 44 (2005) 4391–4395.
[2] J.K. Lee, G.P. Kim, I.K. Song, S.H. Baeck, Electrochem. Commun. 11 (2009) 1571–1574.
[3] J.H. Song, H.J. Park, K.J. Kim, Y.N. Jo, J.S. Kim, Y.U. Jeong, Y.J. Kim, J. Power Sources 195 (2010) 6157–6161.
[4] J. Jiang, Z.X. Wang, L.Q. Chen, J. Phys. Chem. C 111 (2007) 10707–10711.
[5] M.E. Spahr, P. Novák, W. Scheifele, O. Haas, R. Nesper, J. Electrochem. Soc. 145 (1998) 421–427.
[6] C.C. Torardi, C.R. Miao, Chem. Mater. 14 (2002) 4430–4433.
[7] S. Panero, M. Pasquali, G. Pistoia, J. Electrochem. Soc. 130 (1983) 1225–1227.
[8] H.Y. Xu, H. Wang, Z.Q. Song, Y.W. Wang, H. Yan, M. Yoshimura, Electrochim. Acta 49 (2004) 349–353.
[9] G. Pistoia, S. Panero, M. Tocci, R. Moshtev, V. Manev, Solid State Ionics 13 (1984) 311–318.
[10] H.M. Liu, Y.G. Wang, K.X. Wang, Y.R. Wang, H.S. Zhou, J. Power Sources 192 (2009) 668–673.
[11] N.A. Chernova, M. Roppolo, A.C. Dillon, M.S. Whittingham, J. Mater. Chem. 19 (2009) 2526–2552.
[12] G.Q. Liu, C.L. Zeng, K. Yang, Electrochim. Acta 47 (2002) 3239–3243.
[13] P.G. Bruce, B. Scrosati, J.M. Tarascon, Angew. Chem. Int. Ed. 47 (2008) 2930–2946.
[14] Z.S. Hong, M.D. Wei, X.K. Ding, L.L. Jiang, K.M. Wei, Electrochem. Commun. 12 (2010) 720–723.
[15] X. Wang, Y.D. Li, J. Am. Chem. Soc. 124 (2002) 2880–2881.
[16] Y.G. Li, B. Tan, Y.Y. Wu, Nano Lett. 8 (2008) 265–270.
[17] G.C. Li, S.P. Pang, L. Jiang, Z.Y. Guo, Z.K. Zhang, J. Phys. Chem. B 110 (2006) 9383–9386.
[18] R.Z. Ma, Y. Bando, L.Q. Zhang, T. Sasaki, Adv. Mater. 16 (2004) 918–922.
[19] H.Y. Wang, K.L. Huang, S.Q. Liu, C.H. Huang, W.J. Wang, Y. Ren, J. Power Sources 196 (2011) 788–792.
[20] S.D. Huang, Y.K. Shan, Chem. Commun. (1998) 1069–1070.
[21] H.M. Liu, Y.G. Wang, L. Li, K.X. Wang, E. Hosonoa, H.S. Zhou, J. Mater. Chem. 19 (2009) 7885–7891.
[22] P.N. Trikalitis, V. Petkov, M.G. Kanatzidis, Chem. Mater. 15 (2003) 3337–3342.
[23] X.C. Wu, Y.R. Tao, L. Dong, J.M. Hong, J. Mater. Chem. 14 (2004) 901–904.
[24] K.F. Zhang, G.Q. Zhang, X. Liu, Z.X. Su, H.L. Li, J. Power Sources 157 (2006) 528–532.
[25] B. Azambre, M.J. Hudson, O. Heintz, J. Mater. Chem. 13 (2003) 385–389.
[26] A. Dobley, K. Ngala, S.F. Yang, P.Y. Zavalij, M.S. Whittingham, Chem. Mater. 13 (2001) 4382–4386.
[27] K.S. Lee, S.T. Myung, J.S. Moon, Y.K. Sun, Electrochim. Acta 53 (2008) 6033–6037.
[28] Y. Makimura, T. Ohzuku, J. Power Sources 119–121 (2003) 156–169.
[29] F.P. Koffyberg, F.A. Benko, Philos. Mag. B 38 (1978) 357–366.
[30] H.Y. Wang, A.D. Tang, K.L. Huang, S.Q. Liu, Trans. Nonferrous Met. Soc. China 20 (2010) 803–808.
[31] Y.J. Kang, J.H. Kim, S.W. Lee, Y.K. Sun, Electrochim. Acta 50 (2005) 4784–4791.
[32] A.J. Bard, L.R. Faulkner, Electrochemical Methods, seconded., Wiley, 2001, p. 231.
[33] A.Y. Shenouda, H.K. Liu, J. Power Sources 185 (2008) 1386–1391.
[34] Q. Cao, H.P. Zhang, G.J. Wang, Q. Xia, Y.P. Wu, H.Q. Wu, Electrochem. Commun. 9 (2007) 1228–1232.